Advances in Nano Research, *Vol. 14, No. 4 (2023) 313-327*
https://doi.org/10.12989/anr.2023.14.4.313

Highly catalysis Zinc MOF-loaded nanogold coupled with aptamer to assay trace carbendazim by SERS

Jinling Shi, Jingjing Li, Aihui Liang and Zhiliang Jiang*

Guangxi Key Laboratory of Environmental Pollution Control Theory and Technology, Key Laboratory of Ecology of Rare and Endangered Species and Environmental Protection (Guangxi Normal University), Ministry of Education, Guilin 541004, China

(*Received November 2, 2021, Revised November 8, 2022, Accepted November 17, 2022*)

Abstract. Zinc metal organic framework (MOF_{Zn})-loaded goad nanoparticles (AuNPs) sol ($Au@MOF_{Zn}$), which was characterized by TEM, Mapping, FTIR, XRD, and molecular spectrum, was prepared conveniently by solvothermal method. The results indicated that $Au@MOF_{Zn}$ had a very strong catalytic effect with the nanoreaction of AuNPs formation between sodium oxalate (SO) and HAuCl4. AuNPs in the new indicator reaction had a strong resonance Rayleigh scattering (RRS) signal at 370 nm. The indicator AuNPs generated by this reaction, which had the most intense surface enhanced Raman scattering (SERS) peak at 1621 cm -1. The new SERS/RRS indicator reaction in combination with specific aptamer (Apt) to fabricate a sensitive and selective $Au@MOF_{Zn}$ catalytic amplification-aptamer SERS/RRS assay platform for carbendazim (CBZ), with SERS/RRS linear range of 0.025-0.5 ng/mL. The detection limit was 0.02 ng/mL. Similarly, this assay platform has been also utilized to detect oxytetracycline (OTC) and profenofos (PF).
Keywords: $Au@MOF_{Zn}$ nanocatalytic amplification; AuNP dimode indicator reaction; Apt; SERS; RRS

1. Introduction

Metal organic framework (MOF) was a three-dimensional framework material with microporous structure synthesized by spontaneous assembly of metal salt as the central ion and organic ligand through coordination bonds. With well-defined pores and a large specific surface area, as well as homogeneous catalytic active sites, MOF could certainly be used as catalysts under the right conditions. We also knew that metal nanoparticles were also an efficient catalyst. Metal nanoparticles had a catalytic effect due to their small particle size, resulting in a high specific surface energy, with the disadvantage that they tended to aggregate, which in turn impaired their catalytic ability. Therefore, it is important to find simple, stable, and cheap carriers to prepare metal nanoparticles in order to maintain good stability and high catalytic activity. It has been shown that when MOFs were doped with additional metal particles, in addition to preventing migration and aggregation of metal nanoparticles, the properties and applications of MOFs could be extended, which were reflected in practical applications in chemistry, food, medicine, environmental protection and analytical chemistry. (Veisi *et al*. 2021, Tayyaba *et al*. 2021, Harrison *et al*. 2021) Therefore, the preparation of cheap and stable MOF was of great interest. Currently, the most commonly used method for the preparation of MOF is the solvothermal method, which is simple to operate, has a large number of products and a high success rate compared to other methods. As a matter of course, our first choice for the preparation of MOF_{Zn} was the solvothermal method. Furthermore, the stirring method was a simple and fast preparation method. This method gave the advantage of short time and good results for MOF loaded nanoparticles. The combination of the solvothermal method and the stirring method ensured a high yield of MOF and increased the efficiency. Moreover, as a new nanomaterial, MOF has been applied not only for common electrochemical analysis but also for spectral analysis. An MOF_{Eu} material was prepared by Wu and Yan (2017), which could selectively detect MnO_4^- through fluorescence quenching effect. Shi *et al*. (2015) prepared a MOF that can be used as a luminescent probe to detect I^- in aqueous solutions. Li *et al*. (2017) used $MOF_{Eu/Zr}$ to establish a new fluorescence method for the detection of formaldehyde by the intensity ratio of the dual emission peaks. Tawfik and Lee (2021) demonstrated an easy and convenient sensor based on the new π-conjugated MOF for the detection of 1-hydroxypyrene. Indeed, MOF showed superior performance by loading with other substances. Setoudeh *et al*. (2020) used a nanocomposite composed of cobalt-tannic acid and ZIF-8 for the simultaneous determination of acetaminophen, dopamine, tryptophan, and uric acid. As reported by Dong *et al*. (2017), a new glycine-MIL-53(Fe), which expressed a better peroxidase-like activity for TMB, was rationally designed. The stability of glycine-MIL-53(Fe) was better than that of MIL-53(Fe) under different pH conditions, indicating that the performance of the doped MOF was enhanced. We knew that the specific binding of antibodies, aptamers, or DNA strands could effectively detect the corresponding substances. Ali *et al*. (2020) developed an ultrasensitive electrochemical aptamer sensor for PCB77 detection based on MoS_2-rGO/Thi. Hence, we could try to establish new methods through MOF combined with aptamers and apply them to spectral analysis. For example, MOF_{Ce} could bind specifically to Apt to detect dopamine

*Corresponding author, Professor,
E-mail: zljiang@mailbox.gxnu.edu.cn

ISSN: 2287-237X (Print), 2287-2388 (Online)

with a detection limit of 0.008 nmol/L. (Shi *et al*. 2022) To our knowledge, there were no reports on MOF_{Zn}-loaded nanogold as a catalyst for aptamer (Apt)-mediated catalytic amplification of surface-enhanced Raman scattering and resonant Rayleigh scattering spectra.

Resonant Rayleigh scattering (RRS) was a kind of elastic scattering. RRS method had the benefits of simplicity, good sensitivity as well as excellent selectivity. The RRS method combined with nanomaterials has been applied in biomolecules analysis, heavy metals analysis, environmental analysis, and other fields. For example, gold-doped polystyrene nanoenzyme could be combined with an RRS method for the sensitive detection of glyphosate. The RRS intensity was linearly related to glyphosate over a concentration range of 0.5-20 nmol/L, with a detection limit as low as 0.24 nmol/L. (Wang *et al*. 2022) A RRS method was combined with silver nanocubes for the determination of haloperidol was established by Gheitaran *et al*. (2022), which RRS intensity had a linear relationship with haloperidol within a certain concentration range and the detection limit was 1.5 ng/mL. Surface-enhanced Raman scattering (SERS) was an inelastic scattering with high sensitivity, high selectivity, and other characteristics, which was one of the successful applications of nanomaterials. The study of SERS analysis mainly focused on the detection of heavy metals, organic compounds, and biological macromolecules. For example, Guselnikova *et al*. (2019) made MOF_{Zn} combined with SERS for the measurement of organophosphorus pesticides with a detection limit of 10^{-12} mol/L. A new Ag@Ni-MOF-1 as an integrated SERS platform was designed and developed by Yang *et al*. (2020), which not only successfully catalyzed *in-situ* synthesis of DA-Quinone at physiological pH value but established a specific method to detect cysteine. Last few years, as research has deepened, a series of dual-mode analysis methods have been developed to solve the deficiency of single molecule spectrum and have been applied at biological and environmental aspects. A novel AuBtPD, which combined with nano-catalytic reaction to amplify the double scattering signal of cobalt ions and specific Apt, was prepared by Wen *et al*. (2021), and a two-mode method for detection of Co^{2+} was established. RRS and SERS signal showed a linear relationship with 0.033-1 nmol/L Co^{2+}. Nitrogen/Silver co-doped carbon dot (CDN/Ag) with high catalytic amplification performance was prepared by microwave method. The CDN/Ag catalytic amplification and the specific immune reaction of Clen were combined with SERS and RRS to construct a new double spectral detection strategy. The detection limit of Clen was 0.68 pg/mL. (Yao *et al*. 2020) Yao *et al*. (2020) integrated SERS and RRS method, which based on the AuNPs produced by the catalytic reduction of $HAuCl_4$ by AuNPs as a dual-function probe for SERS and RRS. The dual-mode method could establish to detect 3.0-413 ng/mL CO.

Carbendazim (CBZ) and oxytetracycline (OTC) were a highly effective and low-toxic internal broad-spectrum fungicide, which had protective and therapeutic effects, and had a control effect on a variety of disease crops and has been widely used at home and abroad. At present, commonly used detection methods include immunoassay, liquid chromatography, (Zheng *et al*. 2022, Deng *et al*. 2022, Sakda *et al*. 2020, Alanazi *et al*. 2021) SERS method. A fast and highly sensitive ELISA immunoassay was developed by Song *et al*. (2019), which could detect CBZ in mushroom samples within 1 hour. The linear range was 0.4-58.0 μg/L, and the average recovery was 89.7-112.7%. The CBZ concentration in tea was detect by using SERS by Ma *et al*. (2015) There was a linear relationship between CBZ concentration at 0.5-8 mg/kg and SERS intensity. The content of oxytetracycline in duck meat using the fluorescence intensity generated by a complex of oxytetracycline and europium(III) was detected by Zhao *et al*. (2014). The results showed that the fluorescence signal at the OTC concentration of 0.05-20 mg/L increased linearly, and the detection limit was 0.05mg/L. In this study, based on the specific binding of Apt-CBZ/OTC and the catalytic amplification strategy of Au@MOF_{ZnC}-$HAuCl_4$-sodium oxalate, a sensitive and convenient CBZ/OTC assay platform with SERS and RRS dual-signal was constructed. Compared with most CBZ/OTC detection methods, this method was convenient, efficient, and had higher sensitivity.

2. Experimental

2.1 Instrument

A model of UPW-N15UV Ultra-Pure Water Machine Shanghai Yidian Scientific Instrument Co., Ltd., Shanghai, China), a model of SK3300B sonic clean machine (Shanghai Kudos Ultrasonic Instrument Co., Ltd., Shanghai, China), a model of F-7000 fluorescence spectrophotometer (Haitachi Co., Tokyo, Japan), a model of 79-1 magnetic heating stirrer (Jiangsu University Instrument Factory Co., Ltd., Jiangsu, China), DXR2 Smart Raman Spectrometer (Thermo), a dual-beam UV-visible spectrophotometer with model of TU-1901 (Beijing Puxi General Equipment Limited Co., Beijing, China), a model of HH-S2 constant temperature water bath kettle (Ointan Dadi Automatic Instrument Co., Changzhou, China), an electric thermostatic drying oven (Shanghai Jing Hong Laboratory Instrument Co., Ltd., Shanghai China), and a high-speed freezing centrifuge (Shanghai Lu Xiangyi Centrifuge Instrument Co., Ltd., Shanghai, China) were used.

2.2 Reagent

$HAuCl_4 \cdot 4H_2O$ (Sinopharm Chemical Reagent Co. LTD.); sodium oxalate (SO, Shantou Xilong Chemical Co., LTD.); N, N-dimethylformamide (DMF, Guangdong Guanghua SCI-Tech Co., LTD.); zinc nitrate hexahydrate, trisodium citrate (TC, Xilong Scientific Co., LTD.); carbendazim (CBZ, Sigma-aldrich (Shanghai) Trading Co., LTD.); oxytetracycline aptamer (Apt_o, CGA CGC ACA GTC GCT GGT GCG TAC CTG GTT GCC GTT GTG T) (Wang *et al*. 2020), oxytetracycline hydrochloride (OTC), carbendazim aptamer (Apt_c, GGG CAC ACA ACA ACC GAT GGT CCA GCC ACC CGA ATG ACC AGC CCA

CCC GCC ACC CCG CG) (Bahreyni *et al*. 2020), profenofos aptamer (Apt_{PF}, AAG CTT GCT TTA TAG CCT GCA GCG ATT CTT GAT CGG AAA AGG CTG AGA GCT ACG C) (Shi *et al*. 2021) (Shanghai Shenggong Biological Engineering Co., LTD.); terephthalic acid (H_2BDC), profenofos (Shanghai McLean Biochemical Technology Co., LTD.) were used, all the above drugs were analytically pure, and the experimental water was deionized water.

2.3 Preparation of Au@MOF$_{Zn}$

MOF_{Zn}: 2.42 g zinc nitrate hexahydrate (8.13mmol), 0.67g terephthalic acid (4.03mmol) and 40.0 mL DMF were mixed in a high temperature reaction kettle lined with polytetrafluoroethylene material and placed in a constant temperature chamber at 120 ℃ for 24 h. After completion of the reaction, the solution was cooled to room temperature to obtain a white solution, which was washed three times with DMF solution and deionized water, and high-speed freezing centrifugation (10000 r/min, 10 min) was used to obtain pure white solid. In the end, the product was dried at 75 ℃ for 24 h to obtain a white solid. (Wu *et al*. 2014) Cu, Co, and Zn were metal elements of the same main family in the periodic table of elements, and the MOF_{Cu} and MOF_{Co} were used in previous experiments, but the results were not ideal. The MOF_{Cu} powder prepared by solvothermal method was blue. After adding water and ultrasound, the powder was easily combined with water to form floccule, so further experiments could not be carried out. The MOF_{Co} powder prepared by stirring method at room temperature was purple and had good catalytic effect. The disadvantage was that it was very unstable in aqueous solution, and the catalytic effect decreases obviously with time. MOF_{Zn} completely avoided the above shortcomings and could be stably stored in aqueous solution with good catalytic effect.

$AuNP_C$: First 1.0 mL of 0.1 % $HAuCl_4$ was added to 10.0 mL of H_2O and the solution was kept at a boil, then 0.5 mL of 1.0 % TC was slowly added with stirring. The solution was stirred continuously for 15 min and then fixed the volume to 25.0 mL. The concentration of $AuNP_C$ obtained was 23.0 μg/mL.

$Au@MOF_{ZnC}$: First 1.0 mL of 0.1 % $HAuCl_4$ was added to 10.0 mL of 0.1 mg/mL MOF_{Zn} and the solution was kept at a boil, then 0.5 mL of 1.0 % TC was slowly added with stirring. The solution was stirred continuously for 15 min and then fixed the volume to 25.0 mL. The concentration of $Au@MOF_{ZnC}$ obtained was 40.0 μg/mL (calculated as MOF_{Zn}). (Yao *et al*. 2020)

2.4 Experimental methods

Firstly, a certain concentration of targets, 140 μL Apt (0.01 nmol/mL), 30.0 μL $Au@MOF_{ZnC}$ (0.4 μg/mL) were added to a 5.0 mL test tube, mixed well, and let stand for 10 min in 80 ℃. Then 30.0 μL sodium oxalate (10.0 μmol/mL), 120 μL HCl (0.01 mmol/mL), 80.0 μL $HAuCl_4$ (1 mg/mL) were added, and the volume was adjusted to 2.0 mL, and the mixture was uniformly mixed. Finally, the reaction solution was reacted at 80 ℃ for 10 min and then cooled with ice water. The solution was added 70.0 μL 10.0 μmol/L Vitoria blue 4r (VB4r) and were recorded by scanning the solution with Raman spectrometer. The indicator AuNPs generated by this reaction, which had the most intense SERS peak at 1621 cm^{-1} ($I_{1621cm^{-1}}$). Meanwhile, the intensity of blank solution without added targets at 1621 cm^{-1} was recorded as $(I_{1621cm^{-1}})_0$ and calculated $\Delta I_{1621cm^{-1}} = I_{1621cm^{-1}} - (I_{1621cm^{-1}})_0$. Similarly, Fluorescence spectrophotometer obtained that AuNPs had a strong RRS peak at 370 nm ($I_{370\ nm}$) and the blank $(I_{370\ nm})_0$, and calculated $\Delta I_{370\ nm} = I_{370\ nm} - (I_{370\ nm})_0$.

3. Results and discussion

3.1 Analysis principles

$Au@MOF_{ZnC}$ had a strong catalytic effect on SO reducing $HAuCl_4$ to gold nanoparticles and generated strong RRS signal. After added probe VB4R, the system would also produce a strong SERS signal. After added Apt to the system, the contact between the active site on $Au@MOF_{ZnC}$ surface and SO-$HAuCl_4$ was blocked, and the catalytic reaction was inhibited, resulting in a weakening of the RRS/SERS signal. After adding CBZ, because CBZ could specifically combine with its aptamer to form a stable Apt_c-CBZ complex, at this time $Au@MOF_{ZnC}$ was released and the surface-active site was exposed, thus the catalytic effect of $Au@MOF_{ZnC}$ was restored. As the CBZ concentration increased, more $Au@MOF_{ZnC}$ was released. The catalytic reaction of SO-$HAuCl_4$ was accelerated, the concentration of generated AuNPs increased, and the RRS/SERS signal was recovered. In a certain concentration interval, the signal showed a tendency to increase linearly, using this catalytic amplification reaction could establish the RRS/SERS spectral analysis method to detect trace CBZ. (see Fig. 1)

3.2 MOF characterization

To test the stability of MOF_{Zn}, $AuNP_B$, $AuNP_C$, $AuNP_{CO}$, $Au@MOF_{ZnB}$, $Au@MOF_{ZnC}$ and $Au@MOF_{ZnCO}$ in aqueous solutions, their stability in NaCl and signal changes over two weeks were investigated by scanning RRS and Abs spectra respectively. (see Figs. 2(a)-(d)) Finally, MOF_{Zn}, $AuNP_C$ and $Au@MOF_{ZnC}$ were selected as the catalyst to determine OTC and CBZ for this experiment. The results showed that the RRS/Abs signal of MOF_{Zn} could maintain stable for a long time, while $AuNP_C$ had poor stability and tended to aggregate with time. When $AuNP_C$ was combined with MOF_{Zn}, it could be loaded in MOF_{Zn} to improve its stability in aqueous solution. The MOF_{Zn} material provided a stable carrier for AuNPc. The fluorescence characteristics of MOF_{Zn} and $Au@MOF_{ZnC}$ were investigated. The fluorescence peaks of MOF_{Zn} and $Au@MOF_{ZnC}$ were all distributed at 425 nm, and the fluorescence effect was the strongest when the wavelength of excitement was 310 nm. Different concentrations of $Au@MOF_{ZnC}$ and MOF_{Zn} were obtained by dilution with ultrapure water, and their fluorescence spectra were obtained by fixing the excitation

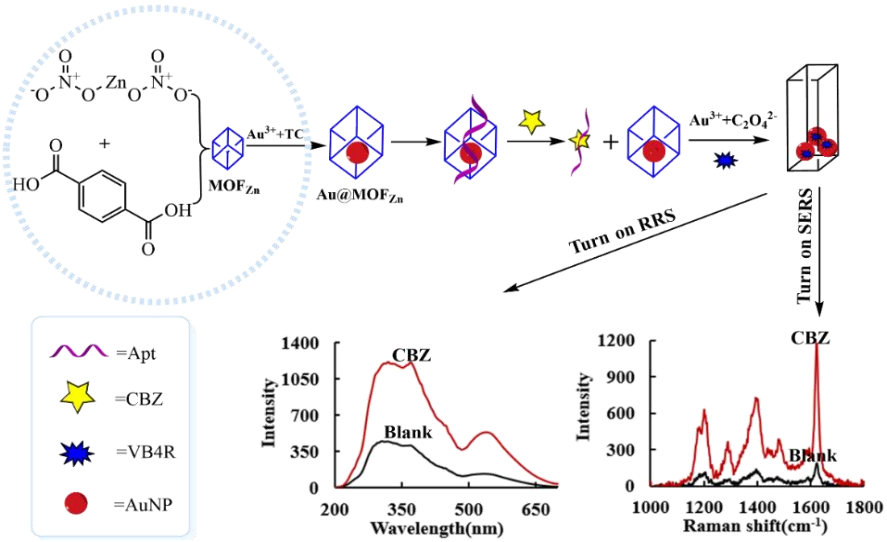

Fig. 1 Schematic diagram of Apt mediating Au@MOF_{ZnC} catalytic amplifying dimode scattering spectral assay for CBZ

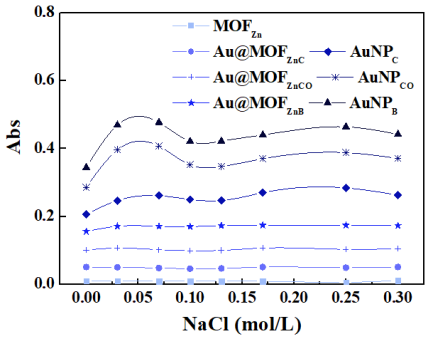

(a) The Abs signal of MOF_{Zn}/$AuNP_B$/$AuNP_C$/ $AuNP_{CO}$/Au@MOF_{ZnB}/Au@MOF_{ZnC}/Au@MOF_{ZnCO} varying with NaCl

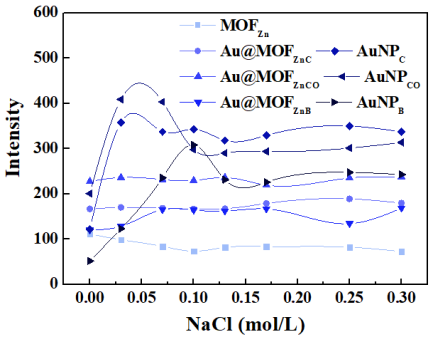

(b) The RRS signal of MOF_{Zn}/$AuNP_B$/$AuNP_C$/ $AuNP_{CO}$/Au@MOF_{ZnB}/Au@MOF_{ZnC}/Au@MOF_{ZnCO} varying with NaCl

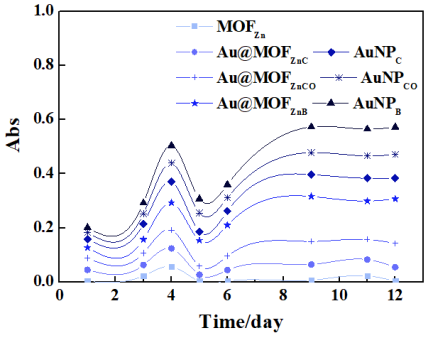

(c) The Abs signal of MOF_{Zn}/$AuNP_B$/$AuNP_C$/ Au@MOF_{ZnB}/$AuNP_{CO}$/Au@MOF_{ZnC}/Au@MOF_{ZnCO} varying with time

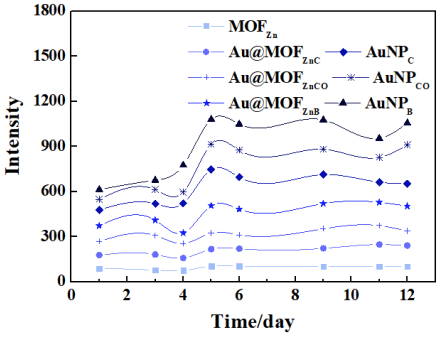

(d) The RRS signal of MOF_{Zn}/$AuNP_B$/$AuNP_C$/ $AuNP_{CO}$/Au@MOF_{ZnB}/Au@MOF_{ZnC}/Au@MOF_{ZnCO} varying with time

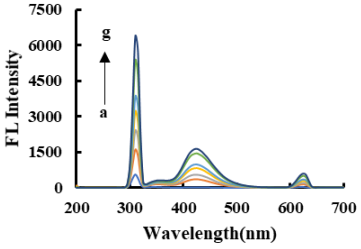

(e) fluorescence spectrum of Au@MOF_{ZnC}: a-g: 0, 0.08, 0.16, 0.2, 0.24, 0.32, 0.4 μg/mL

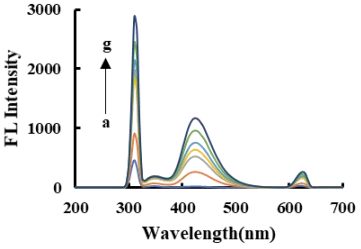

(f) fluorescence spectrum of MOF_{Zn}: a-g: 0, 10, 20, 30, 40, 50, 60 μg/mL

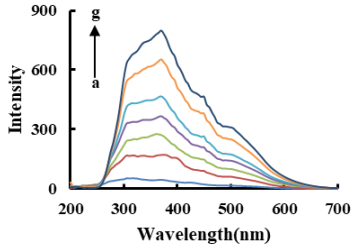

(g) RRS spectrum of MOF_{Zn}:
a-g: 0, 10, 20, 30, 40, 50, 60 μg/mL

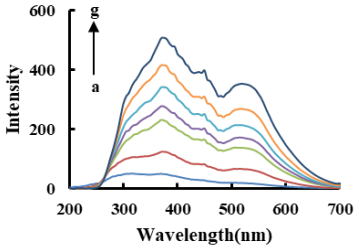

(h) RRS spectrum of $Au@MOF_{ZnC}$:
a-g: 0, 0.08, 0.16, 0.2, 0.24, 0.32, 0.4 μg/mL

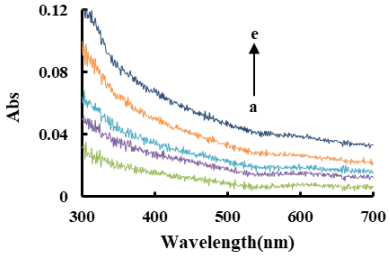

(i) Abs spectrum of MOF_{Zn}:
a-e：0.04, 0.06, 0.08, 1, 1.2 mg/mL

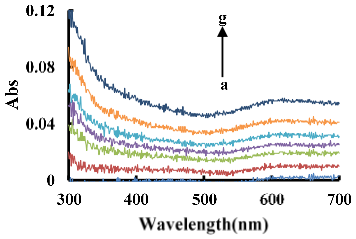

(j) Abs spectrum of $Au@MOF_{ZnC}$:
a-g：0, 0.08, 0.16, 0.2, 0.24, 0.32, 0.4 μg/mL

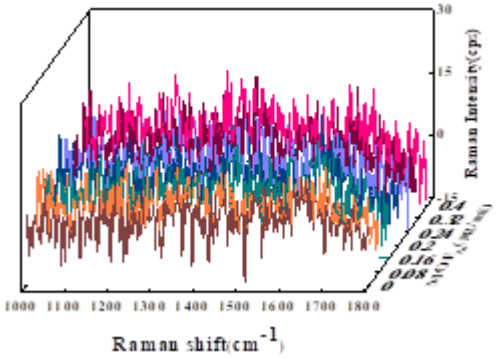

(k) Raman spectrum of MOF_{Zn}+80 nmol/mL AgNPs+2.5 μmol/mL NaCl

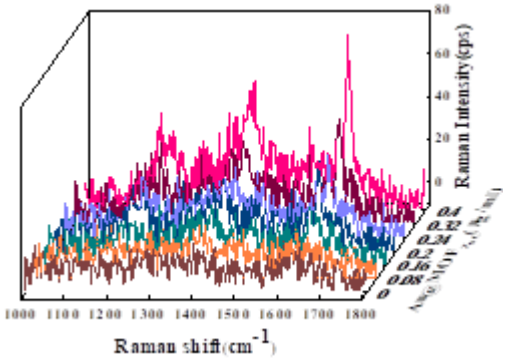

(l) Raman spectrum of $Au@MOF_{ZnC}$+80 nmol/mL AgNPs+2.5 μmol/mL NaCl

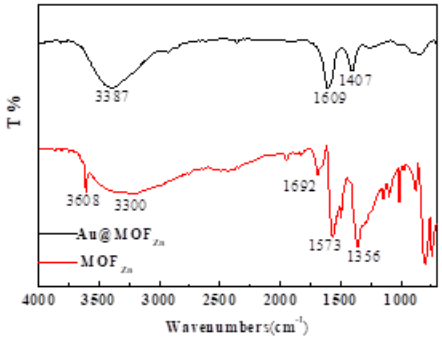

(m) Infrared spectrum of MOF_{Zn} and $Au@MOF_{ZnC}$

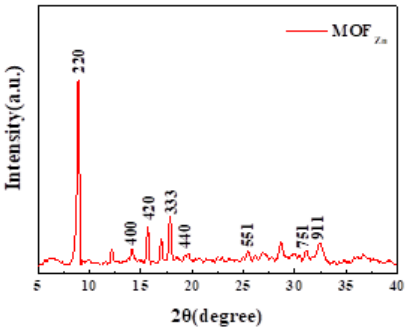

(n) XRD of MOF_{Zn}

Fig. 2 Molecular spectrum of MOF_{Zn}/$Au@MOF_{ZnC}$

wavelength at 310 nm. (see Figs. 2(e)-(f)) Thus, it could be seen that $Au@MOF_{ZnC}$ showed stronger fluorescence behavior than MOF_{Zn}. For the RRS spectra of $Au@MOF_{ZnC}$ and MOF_{Zn} at 370 nm was linearly correlated with the concentration of $Au@MOF_{ZnC}$ and MOF_{Zn}, but the RRS of MOF_{Zn} was not as effective as $Au@MOF_{ZnC}$. This indicates that larger particles were formed during the preparation of $Au@MOF_{ZnC}$. (see Figs. 2(g)-(h)) Figs. 2(i)-(j) showed that both MOF_{Zn} and $Au@MOF_{Zn}$ had wide absorption bands at 300-700 nm, and their absorption progressively increases as the concentration of MOF_{Zn} and $Au@MOF_{ZnC}$ magnify. Using AgNPs as SERS base and NaCl as the sensitizer, we studied the SERS spectra of MOF_{Zn} and $Au@MOF_{ZnC}$, and the results showed that there was no obvious SERS peak. It's indicated that $Au@MOF_{ZnC}$ could not be used as a Raman molecular probe. (see Figs. 2(k)-(l)) Infrared spectra showed that MOF_{Zn} had several characteristic peaks. The fluctuation in the range of 600-1200 cm^{-1} was due to the in-

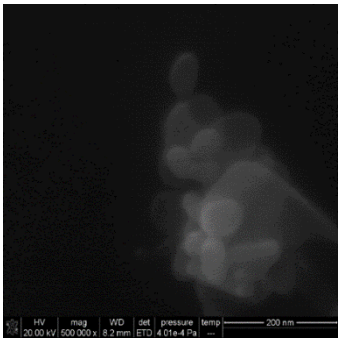

(a) 40.0 μg/mL $HAuCl_4$+0.6 μmol/mL HCl+0.15 μmol/mL SO+6.0 ng/mL Au@MOF_{ZnC} +0.75 pmol/mL Apt_c+0.05 ng/mL CBZ

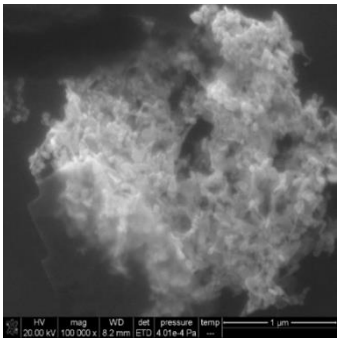

(b) 40.0 μg/mL $HAuCl_4$+0.6 μmol/mL HCl+0.15 μmol/mL SO+6.0 ng/mL Au@MOF_{ZnC} +0.75 pmol/mL Apt_c+0.5 ng/mL CBZ

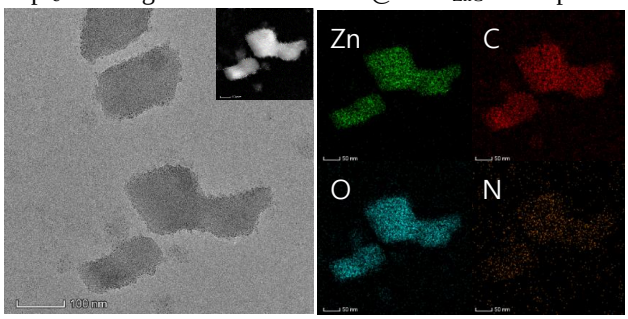

(c) TEM and Mapping of MOF_{Zn}

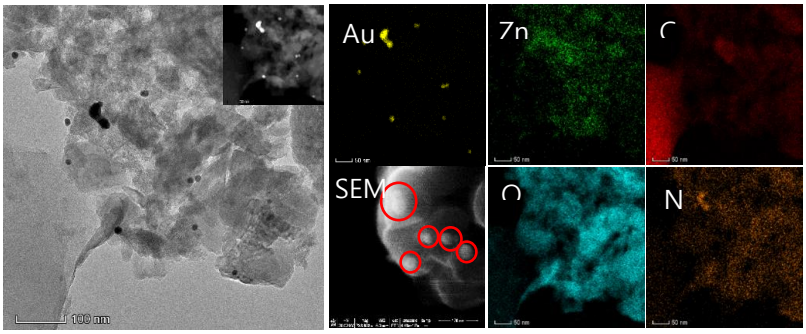

(d) TEM, SEM and Mapping of Au@MOF_{ZnC}

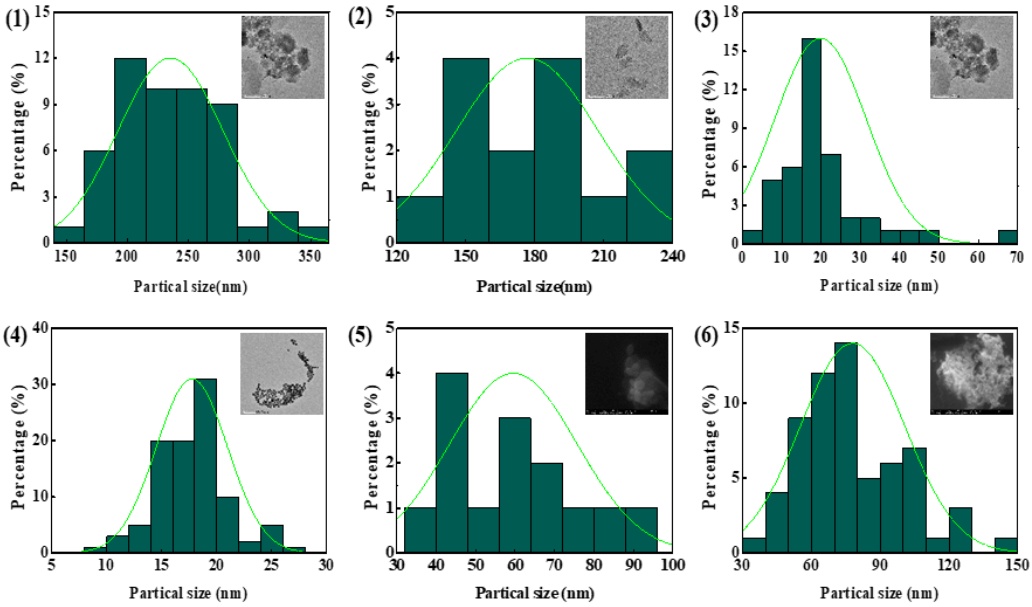

(e) Distribution histogram of the mean particle size;
(1) Au@MOF_{ZnC}, (2) MOF_{Zn}, (3) AuNP in Au@MOF_{ZnC}, (4) $AuNP_C$, (5) AuNP in Fig. 3(a), (6) AuNP in Fig. 3(b).

Fig. 3 Material characterization

plane vibration of phenyl group. Peaks in absorption of 1356 and 1573 cm^{-1} were due to the symmetric and asymmetric elongation vibrations of the carboxylic acid group (-COO) in terephthalic acid (H_2BDC). The absorption peak at 1692 cm^{-1} might be caused by the extended vibration of C=C bond at BDC. Peak in absorption strength of Au@MOF_{ZnC} was different from that of MOF_{Zn} around 3387 cm^{-1}, because the content of crystal water was different, the performance of Au@MOF_{ZnC} in water system was improved, and it had good hydrophilicity and stability. (see Fig. 2(m)) To investigate the crystallinity of the synthesized MOF_{Zn}, it was examined by XRD. It could be seen that the diffraction peaks of 9.2° (220), 13.8° (400), 15.6° (420), 17.8° (333), 19.6° (440), 25.4° (551), 30.8° (751) and 32.5° (911) confirm the crystallinity of the MOF_{Zn}. (see Fig. 2(n)) It was in general agreement with the previous literature. (Anshul *et al*. 2022)

To examine the morphology, size, and distribution of the materials, they were subjected to transmission electron microscopy (TEM) and scanning electron microscope (SEM) tests. The system's reaction liquid was obtained by the experimental method, and the surface of silicon pellet was dropped 20 μL of the reaction liquid. It could be seen by SEM that the amount of AuNPs produced was related to the amount of CBZ added. (see Figs. 3(a)-(b)) In the Mapping diagram we could see that the MOF_{Zn} morphology showed a cubic structure with a more dispersed distribution, while the Au@MOF_{ZnC} profile was not obvious and was concentrated. By comparing the SEM and TEM images of MOF_{Zn} and Au@MOF_{ZnC}, it could be seen that Au@MOF_{ZnC} was indeed loaded with gold nanoparticles. (see Figs. 3(c)-(d)) The average particle size statistics of the materials showed that the average particle size of MOF_{Zn} was 177 nm, while that of Au@MOF_{ZnC} was 240 nm, which showed that the particle size of Au@MOF_{ZnC} has increased after doping with nanogold. The average particle size of $AuNP_C$ was 18 nm, and the average particle size of AuNP in Au@MOF_{ZnC} was 20 nm, indicating that the presence or absence of a carrier had little effect on the particle size of nanogold, but $AuNP_C$ tended to aggregate more. The particle size of the AuNP generated in the analyzed system was generally large and the concentration of targets also influenced the particle size of the gold nanoparticles. (see Fig. 3(e))

3.3 SERS spectra of the catalytic system

SERS is a sensitive molecular spectral technique that was chosen to study the $HAuCl_4$-SO nanoreaction catalyzed by Au@MOF_{ZnC}, $AuNP_C$ and MOF_{Zn}. According to the spectra, the SERS signal of the system raised with increasing catalyst concentration, with a more intuitive signal change at $I_{1621\ cm^{-1}}$. Therefore, the SERS change value of $I_{1621\ cm^{-1}}$ was selected to explore the change of catalytic performance of MOF_{Zn} before and after nanogold-loaded. The catalytic reaction of each material for the reduction of SO by $HAuCl_4$ showed that the slope of MOF_{Zn} was 40.8, the slope of $AuNP_C$ was 14.3 and the slope of Au@MOF_{ZnC} was 226, which far exceeded the sum of the slopes of MOF_{Zn} and $AuNP_C$, thus indicating that the catalytic ability of Au@MOF_{ZnC} was above that of MOF_{Zn}. (see Figs. 4(a)-(c)) In the OTC-Apt_o-Au@MOF_{ZnC}-$HAuCl_4$-SO-HCl system, within 12.5-200 ng/mL concentration range, with the increased of the concentration of OTC, the SERS signal of the system gradually increased. Similarly, the SERS system of MOF_{Zn} and $AuNP_C$ catalytic detection OTC was given as a comparison. It could be visually seen that the signal intensity of the SERS detection system for Au@MOF_{ZnC} was enhanced for the same range of OTC concentrations detected. It could be said that Au@MOF_{ZnC} achieved SERS signal amplification in the detection of OTC systems. (Figs. 4 (d)-(f)) In the aptamer-regulated Au@MOF_{ZnC} catalytic $HAuCl_4$-SO reaction system, the Apt could inhibit catalytic effect. CBZ had a good linear relationship with SERS intensity $\Delta I_{1621\ cm\text{-}1}$ in the range of 0.03-0.5 ng/mL, the linear equation in CBZ-Aptc-Au@MOF_{ZnC}-$HAuCl_4$-SO-HCl detection system was $\Delta I_{1621\ cm\text{-}1}$ = 6488C+160, and the linear equation in CBZ-Aptc-MOF_{Zn}-$HAuCl_4$-SO-HCl detection system was $\Delta I_{1621\ cm\text{-}1}$ = 3901C+157. According to the results given by the equation, Au@MOF_{ZnC} was more advantageous in the determination of CBZ in the same concentration range because of its catalytic effect and SERS signal amplification ability. The same conclusion was reached by Au@MOF_{ZnC} in the system for the determination of PF. (Figs. 4 (g)-(j))

3.4 RRS spectra of the catalytic system

RRS is a simple and sensitive molecular spectral technique that was also selected to investigate the nano-catalytic reaction. The catalysis of Au@MOF_{ZnC}, $AuNP_C$ and MOF_{Zn} on the reaction was studied by RRS, and Au@MOF_{ZnC} had a strongest catalysis on this kind of nanoreaction by the slope of $\Delta I_{370\ nm}$ versus nanoparticle concentration (see Figs. 5(a)-(c)). The system had the largest and most regular peak at 370 nm, so the $I_{370\ nm}$ peak was chosen for measurement. For the $HAuCl_4$-SO-HCl-Au@MOF_{ZnC} system, as the amount of Au@MOF_{ZnC} grown in number, its catalysis and the generated AuNPs progressively enhanced, and the RRS signal intensity in $\Delta I_{370\ nm}$ enhanced. For the Au@MOF_{ZnC}-$HAuCl_4$-SO-HCl-Apt_c nano catalytic analysis system, the Apt_c could be attached to the surface of Au@MOF_{ZnC} by electrostatic attraction to suppress catalysis. When CBZ was added, Apt combined with targets and desorbed from Au@MOF_{ZnC}, and the catalytic capability recovery of Au@MOF_{ZnC}. There was an excellent linearity between $\Delta I_{370\ nm}$ and the target concentration, therefore this peak was chosen to determine targets including CBZ, OTC and PF. (see Figs. 5(d)-(f)) In the aptamer-regulated Au@MOF_{ZnC} catalytic $HAuCl_4$-SO reaction system, the Apt could inhibit catalytic effect. CBZ had a good linear relationship with RRS intensity $\Delta I_{370\ nm}$ in the range of 0.03-0.5 ng/mL, the linear equation in CBZ-Aptc-Au@MOF_{ZnC}-$HAuCl_4$-SO-HCl detection system was $\Delta I_{370\ nm}$ = 1451C+68.3, and the linear equation in CBZ-Aptc-MOF_{Zn}-$HAuCl_4$-SO-HCl detection system was $\Delta I_{370\ nm}$ = 1116C+29.5. According to the results given by the equation, Au@MOF_{ZnC} was more advantageous in the determination of CBZ in the same concentration range because of its catalytic effect and SERS signal amplification

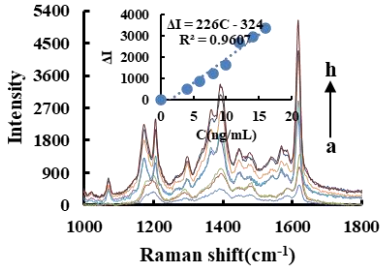

(a) $HAuCl_4$-SO-Au@MOF_{ZnC}-VB4R system, the a-h represent 0, 4.0, 6.0, 8.0, 10.0, 12.0, 14.0 and 16.0 ng/mL Au@MOF_{ZnC}

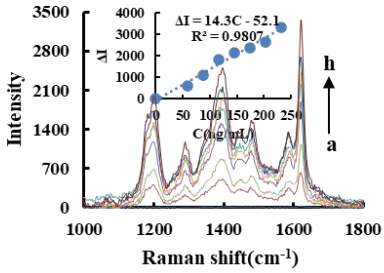

(b) $HAuCl_4$-SO-Au-VB4R system, the a-h represent 0, 58.0, 87.0, 116, 145, 174, 203 and 232 ng/mL Au

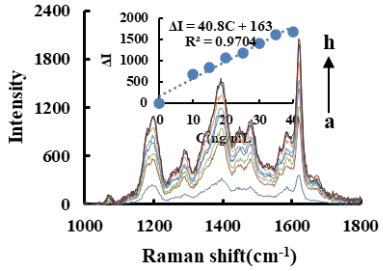

(c) $HAuCl_4$-SO-MOF_{Zn}-VB4R system, the a-h represent 0, 10.0, 15.0, 20.0, 25.0, 30.0, 35.0 and 40.0 ng/mL MOF_{Zn}

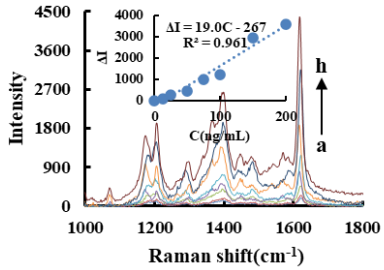

(d) $HAuCl_4$-SO-6.0 ng/mL Au@MOF_{ZnC}-6.25 pmol/mL Apt_o-OTC-VB4R system, the a-h represent 0, 12.5, 25.0, 50.0, 75.0, 100, 150 and 200 ng/mL OTC

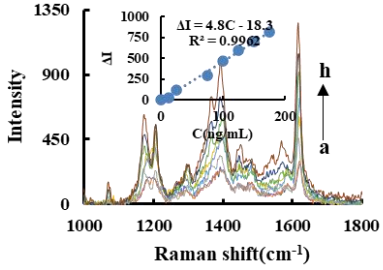

(e) $HAuCl_4$-SO-145 ng/mL Au-12.5 pmol/mL Apt_o-OTC-VB4R system, the a-h represent 0, 12.5, 25.0, 75.0, 100, 125, 150 and 175 ng/mL OTC

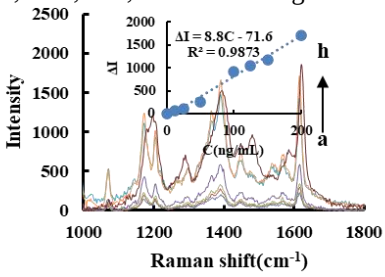

(f) $HAuCl_4$-SO-15.0 ng/mL MOF_{Zn}-1.25 pmol/mL Apt_o-OTC-VB4R system, the a-h represent 0, 12.5, 25.0, 50.0, 100, 125, 150 and 200 ng/mL OTC

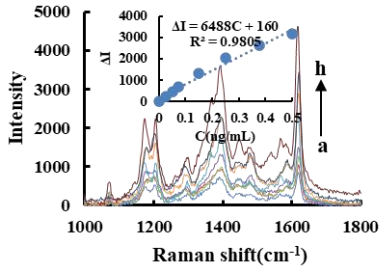

(g) $HAuCl_4$-SO-6.0 ng/mL Au@MOF_{ZnC}-0.75 pmol/mL Apt_c-CBZ-VB4R system, the a-h represent 0, 0.025, 0.05, 0.08, 0.15, 0.25, 0.38 and 0.5 ng/mL CBZ

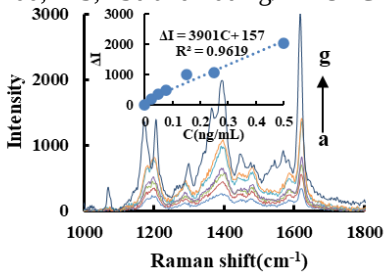

(h) $HAuCl_4$-SO-15.0 ng/mL MOF_{Zn}-0.75 pmol/mL Apt_c-CBZ-VB4R system, the a-g represent 0, 0.025, 0.05, 0.08, 0.15, 0.25 and 0.5 ng/mL CBZ

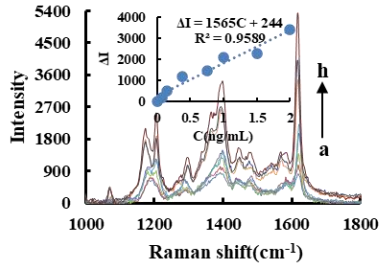

(i) $HAuCl_4$-SO-6.0 ng/mL Au@MOF_{ZnC}-1.25 pmol/mL Apt_{PF}-PF-VB4R system, the a-h represent 0, 0.08, 0.15, 0.38, 0.75, 1.0, 1.5 and 2.0 ng/mL PF

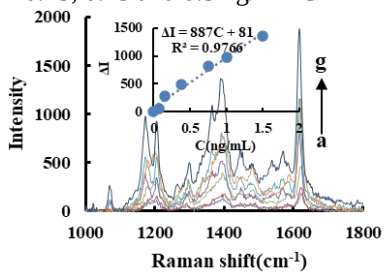

(j) $HAuCl_4$-SO-15.0 ng/mL MOF_{Zn} -1.25 pmol/mL Apt_{PF}-PF-VB4R system, the a-h represent 0, 0.08, 0.15, 0.38, 0.75, 1.0 and 1.5 ng/mL PF

Fig. 4 SERS spectra of $HAuCl_4$-SO reaction system

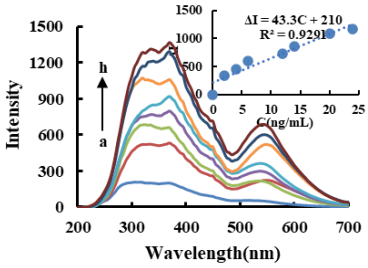

(a) $HAuCl_4$-SO-Au@MOF_{ZnC} system, the a-h represent 0, 2.0, 4.0, 6.0, 12.0, 14.0, 20.0 and 24.0 ng/mL Au@MOF_{ZnC}

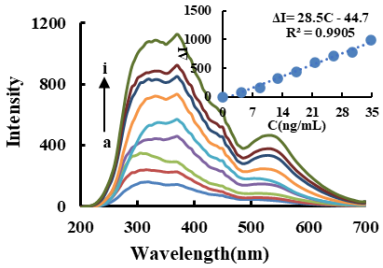

(b) $HAuCl_4$-SO-Au system, the a-i represent 0, 4.4, 8.7, 13.1, 17.4, 21.8, 26.1, 30.5 and 34.8 ng/mL Au

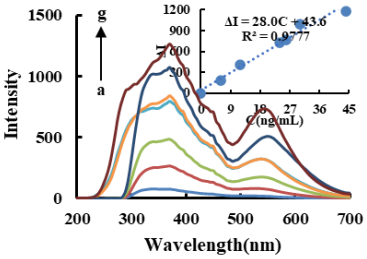

(c) $HAuCl_4$-SO-MOF_{Zn} system, the a-g represent 0, 6.0, 12.0, 24.0,26.0, 30.0 and 44.0 ng/mL MOF_{Zn}

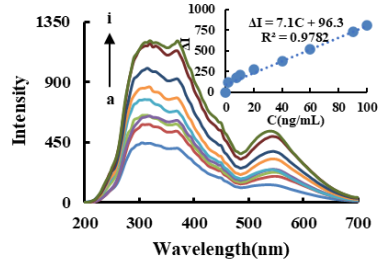

(d) $HAuCl_4$-SO-6.0 ng/mL Au@MOF_{ZnC}-6.25 pmol/mL Apt_o-OTC system, the a-i represent 0, 2.0, 7.5, 10.0, 20.0, 40.0, 60.0, 90.0 and 100 ng/mL OTC

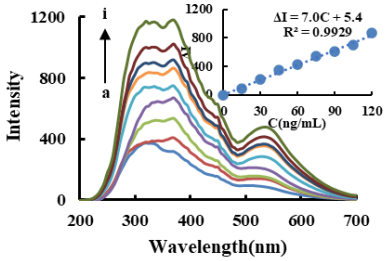

(e) $HAuCl_4$-SO-34.8 ng/mL Au-7.5 pmol/mL Apt_o-OTC system, the a-i represent 0, 15.0, 30.0, 45.0, 60.0, 75.0, 90.0, 105 and 120 ng/mL OTC

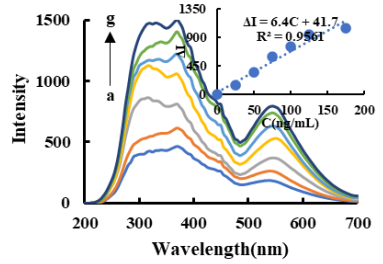

(f) $HAuCl_4$-SO-44.0 ng/mL MOF_{Zn}-5.0 pmol/mL Apt_o-OTC system, the a-h represent 0, 25.0, 50.0, 75.0, 100, 125 and 175 ng/mL OTC

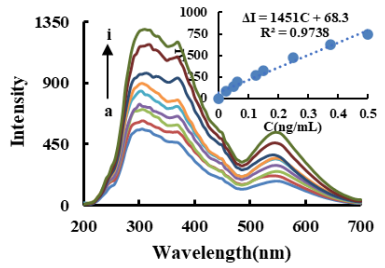

(g) $HAuCl_4$-SO-6.0 ng/mL Au@MOF_{ZnC}-0.75 pmol/mL Apt_c-CBZ system, the a-i represent 0, 0.025, 0.05, 0.06, 0.13, 0.15, 0.25, 0.38 and 0.5 ng/mL CBZ

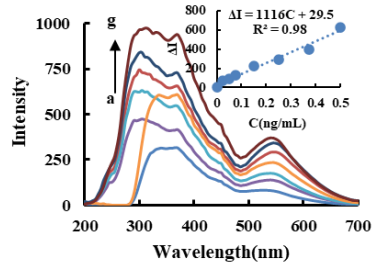

(h) $HAuCl_4$-SO-44.0 ng/mL MOF_{Zn}-1.25 pmol/mL Apt_c-CBZ system, the a-g represent 0, 0.025, 0.05, 0.075, 0.15, 0.25, 0.38 and 0.5 ng/mL CBZ

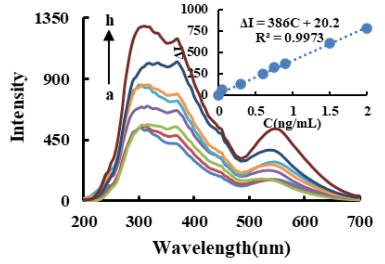

(i) $HAuCl_4$-SO-6.0 ng/mL Au@MOF_{ZnC}-3.75 pmol/mL Apt_{PF} -PF system, the a-h represent 0, 0.05, 0.3, 0.6, 0.75, 0.9, 1.5 and 2.0 ng/mL PF

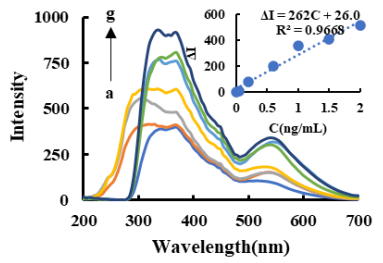

(j) $HAuCl_4$-SO-44.0 ng/mL MOF_{Zn}-3.75 pmol/mL Apt_{PF} -PF system, the a-h represent 0, 0.05, 0.3, 0.6, 0.75, 0.9, 1.5 and 2.0 ng/mL PF

Fig. 5 RRS spectrum of $HAuCl_4$-SO reaction system

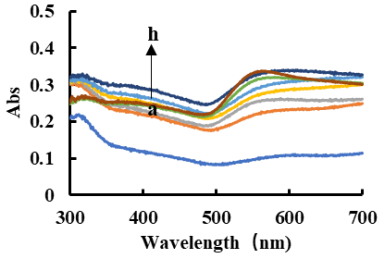

(a) $HAuCl_4$-SO-$Au@MOF_{ZnC}$ system, the a-h represent 0, 0.5, 1.0, 2.0, 4.0, 6.0, 8.0 and 12.0 ng/mL $Au@MOF_{ZnC}$

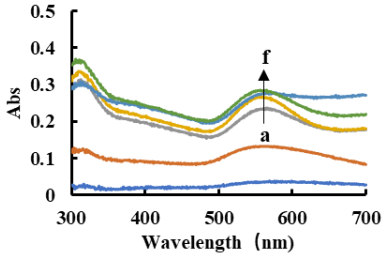

(b) $HAuCl_4$-SO-MOF_{Zn} system, the a-g represent 0, 5.0, 10.0, 15.0, 20.0 and 30.0 ng/mL MOF_{Zn}

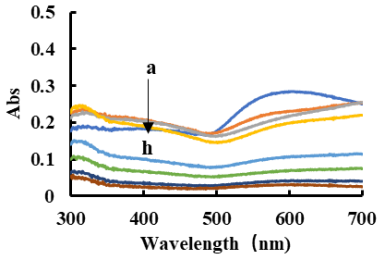

(c) $HAuCl_4$-SO-6.0 ng/mL $Au@MOF_{ZnC}$-Apt_o system, the a-h represent 0, 2.5, 3.75, 5.0, 6.25, 7.5, 8.75 and 10.0 pmol/mL Apt_o.

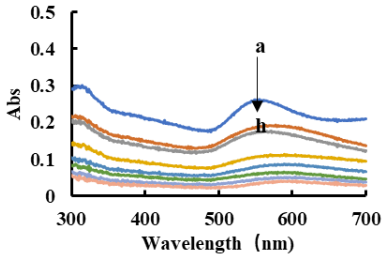

(d) $HAuCl_4$-SO-15 ng/mL MOF_{Zn}-Apt_o system, the a-h represent 0, 1.25, 2.5, 3.5, 5.0, 6.25, 7.5 and 8.75 pmol/mL Apt_o.

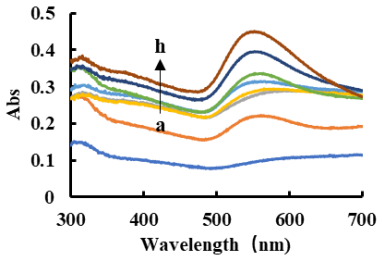

(e) $HAuCl_4$-SO-6.0 ng/mL $Au@MOF_{ZnC}$-6.25 pmol/mL Apt_o-OTC system, the a-h represent 0, 12.5, 25.0, 50.0, 75.0, 100, 150 and 200 ng/mL OTC

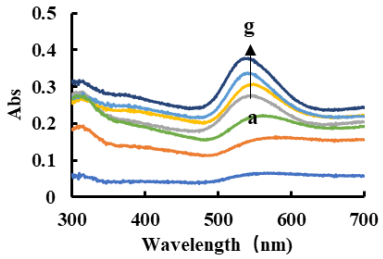

(f) $HAuCl_4$-SO-15.0 ng/mL MOF_{Zn}-5.0 pmol/mL Apt_o-OTC system, the a-g represent 0, 25.0, 50.0, 75.0, 100, 150 and 200 ng/mL OTC

Fig. 6 Absorption spectrum of $HAuCl_4$-SO reaction system

ability. The same conclusion was reached by $Au@MOF_{ZnC}$ in the system for the determination of PF. (see Figs. 5(g)-(j))

3.5 Ultraviolet absorption spectra of the catalysis

Absorption spectroscopy is a simple and low-cost detection technique that has also been used to study nanogold indicator reactions with a surface plasmon resonance absorption peak at around 550 nm. Both $Au@MOF_{ZnC}$ and MOF_{Zn} accelerated the reduction of $HAuCl_4$ by SO, however $Au@MOF_{ZnC}$ achieved an Abs signal closed to that of MOF_{Zn} at lower concentrations, which could indirectly indicate a more intense catalytic ability of $Au@MOF_{ZnC}$. (See Figs. 6(a) and 6(b)) Taking $Au@MOF_{ZnC}$ as an example, in the presence of aptamer, $Au@MOF_{ZnC}$ bound to Apt_o and the catalytic effect of $Au@MOF_{ZnC}$ was inhibited, which was directly reflected in the decrease of Abs signal at 550 nm with the increase of Apt_o concentration. When different concentrations of OTC were added, Apt_o bound to OTC, and $Au@MOF_{ZnC}$ recovered its catalytic activity and catalyzed the rapid release of gold nanoparticles from the $HAuCl_4$-SO system. (See Figs. 6(c) and6(d)). As the concentration of OTC increased, more gold nanoparticles were released and the absorption peak at 550 nm followed. It was observed from Abs spectra that both $Au@MOF_{ZnC}$ and MOF_{Zn} could acted as catalysts for redox reactions, and in the analytical results of detecting the same concentration range of OTC, it was seen that $Au@MOF_{ZnC}$ had the advantage of signal amplification over MOF_{Zn}. (See Figs. 6(e) and 6(f)).

3.6 Catalytic enhancement mechanism of $Au@MOF_{ZnC}$

$HAuCl_4$ and SO undergone a redox reaction in which Au^{3+} was reduced to Au and $C_2O_4^{2-}$ was oxidized to CO_2. The $HAuCl_4$-SO reaction was catalyzed by MOF_{Zn}, AuNPc and $Au@MOF_{Znc}$, ect (see Fig. 7). As a transition element, Au itself had unfilled d-orbital electrons, which were easy to lose or gain in chemical reactions, so it had strong catalytic activity, but AuNPc were unstable and tended to aggregate. MOF_{Zn} was rich in pores, large π bonds and π electrons, which could activate reactants and promote electron transfer. The stability and catalytic activity of

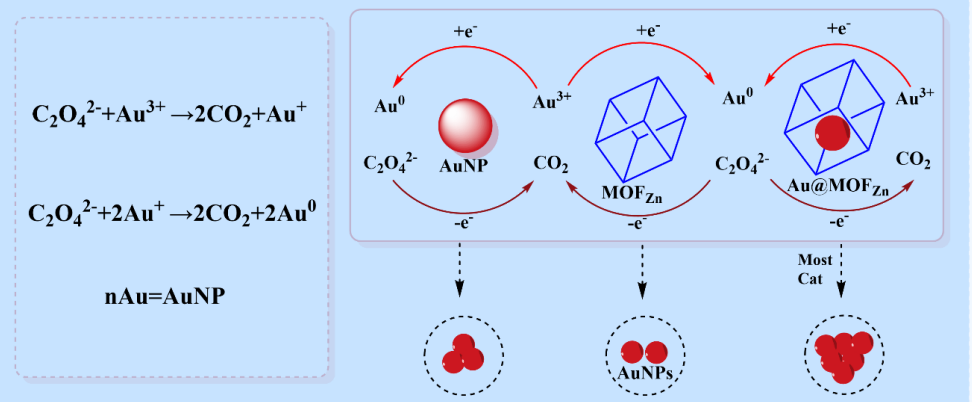

Fig. 7 Catalytic enhancement mechanism of Au@MOF_{ZnC}

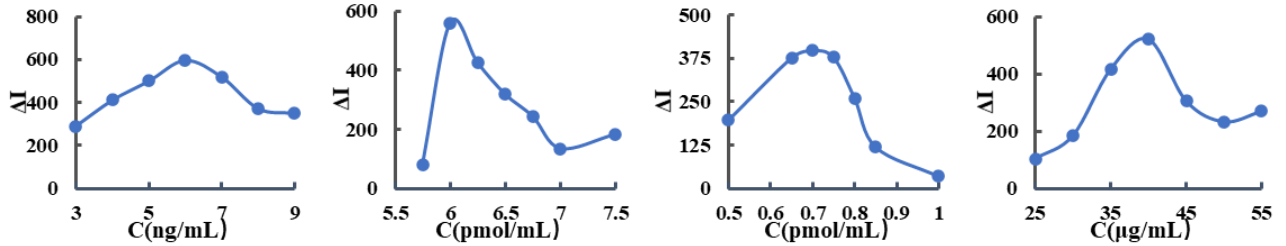

(a) Effect of the concentration of Au@MOF_{ZnC}: Au@MOF_{ZnC}+40 μg/mL $HAuCl_4$+0.6 μmol/mL HCl +0.15 μmol/mL S+6.5 pmol/mL Apt_o+50 ng/mL OTC

(b) Effects of the concentrations of Apt_o: 40 μg/mL $HAuCl_4$+0.6 μmol/mL HCl+0.15 μmol/mL SO+6 ng/mL Au@MOF_{ZnC} +Apt_o+50 ng/mL OTC

(c) Effects of the concentrations of Apt_c: 40 μg/mL $HAuCl_4$+0.6 μmol/mL HCl+0.15 μmol/mL SO+6 ng/mL Au@MOF_{ZnC} +Apt_c+50 ng/mL CBZ

(d) Effects of the concentrations of $HAuCl_4$: $HAuCl_4$+6 ng/mL Au@MOF_{ZnC}+0.6 μmol/mL HCl+0.15 μmol/mL SO+6 pmol/mL Apt_o+50 ng/mL OTC

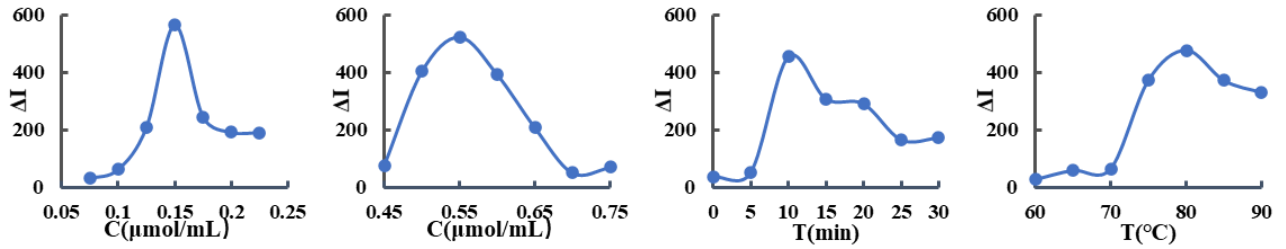

(e) Effects of the concentrations of SO: SO+6 ng/mL Au@MOF_{ZnC}+40 μg/mL $HAuCl_4$+0.6 μmol/mL HCl+6 pmol/mL Apt_o+50 ng/mL OTC

(f) Effects of the concentrations of HCl: HCl+6 ng/mL Au@MOF_{ZnC}+40 μg/mL $HAuCl_4$+0.15 μmol/mL SO+6 pmol/mL Apt_o+50 ng/mL OTC

(g) Effect of heating time on system ΔI: 6 ng/mL Au@MOF_{ZnC}+40 μg/mL $HAuCl_4$+0.55 μmol/mL HCl +0.15 μmol/mL SO+6 pmol/mL Apt_o+50 ng/mL OTC

(h) Effect of temperature on system ΔI: 6 ng/mL Au@MOF_{ZnC}+40 μg/mL $HAuCl_4$+0.55 μmol/mL HCl +0.15 μmol/mL SO+6 pmol/mL Apt_o+50 ng/mL OTC

Fig. 8 Optimized RRS conditions of the target-Apt-$HAuCl_4$-SO-HCl-Au@MOF_{ZnC} reaction system

AuNPc could be improved by loading AuNPc on MOF_{Zn} surface. The coupling of free electron e on Au surface and π electron on MOF_{Zn} surface could promote the electron transfer in the redox reaction of $HAuCl_4$-SO, accelerate the formation of AuNP, and greatly enhance the catalytic activity.

3.8 Working curve

The working curve of the system was drawn depending to the test method. Within a certain range, the target concentration of the target-Apt-$HAuCl_4$-SO-HCl-Au@MOF_{ZnC} system had a linear relationship with the ΔI. The concentration of CBZ with 0.03-0.5ng/mL showed well linear relationship in the RRS peak at $\Delta I_{370\ nm}$ and the SERS peak at $\Delta I_{1621\ cm^{-1}}$. By changing the aptamer, an assay for carbendazim, PF, and OTC could be established (see Table 1). Compared with other reported methods (see Table 2, Eqs. (1)-(3)), the RRS/SERS method established to detect CBZ in this experiment had the advantages of simple operation, high sensitivity, and good selectivity.

$$LOD=3\times\frac{S_b}{K} \quad (1)$$

$$S_b=\sqrt{\frac{1}{n\text{-}1}\sum_{i=1}^{n}(X_i\text{-}\overline{X})^2} \quad (2)$$

S_b—Standard deviation of 11 SERS/RRS signals for the

Table 1 Catalytic effect of MOF on $HAuCl_4$-SO reaction

Materials	Linear range	Regression equation	R^2
MOF_{Zn}	6-30 ng/mL	$\Delta I_{370\ nm}$ =33.5C-16.2	0.9840
$AuNP_B$	4.4-34.8 ng/mL	$\Delta I_{370\ nm}$ =28.5C-44.7	0.9905
$AuNP_{CO}$	6-30 ng/mL	$\Delta I_{370\ nm}$ =28.1C-28.6	0.9868
$AuNP_C$	4-30 ng/mL	$\Delta I_{370\ nm}$ =21.4C+73.3	0.9645
$Au@MOF_{ZnB}$	6-36 ng/mL	$\Delta I_{370\ nm}$ =20.2C-12.5	0.9980
$Au@MOF_{ZnB}$*	3.5-20.9 ng/mL	$\Delta I_{370\ nm}$ =34.8C-12.5	0.9980
$Au@MOF_{ZnC}$	4-16 ng/mL	$\Delta I_{370\ nm}$ =43.3C+210.1	0.9035
$Au@MOF_{ZnC}$*	1.2-13.9 ng/mL	$\Delta I_{370\ nm}$ =74.7C+210.1	0.9035
$Au@MOF_{ZnCO}$	6-22 ng/mL	$\Delta I_{370\ nm}$ =35.5C-15.8	0.9876
$Au@MOF_{ZnCO}$*	3.5-12.8 ng/mL	$\Delta I_{370\ nm}$ = 61.2C-15.8	0.9876

*Calculated as Au

Table 2 Comparison of reported CBZ analysis methods

Method	Principle	Linear range	LOD	Comments	Ref.
Voltammetry	The research involves the synthesis of MIP (molecular-imprinted polymer) of CBZ using methacrylic acid in chloroform as pore-forming agent. It was proved that CBZ MIP was incorporated into CP (carbon paste) electrode as a platform for MIP-CP sensor to detect CBZ.	0.1-100 μmol/L	31 nmol/L	Wide detect range, but cumbersome substrate synthesis	Ghorbani *et al*. (2021)
Colorimetry	A sensitive and selective colorimetric method for the detection of CBZ bactericide in water and food samples was developed by using 4-aminobenthiol functionalized silver nanoparticles (ABT-AgNPs) as colorimetric sensors. Abt-ag NPs, as the CBZ binding probe, interacts with π -π through strong ion pairs to form a huge conjugate network, which changes from yellow to orange in color and is easily visible to the naked eye.	10-100 μmol/L	1.04 μmol/L	Good reproducibility and accuracy, but low sensitivity	Gaurang *et al*. (2015)
Thin-layer chromato -graphy	A combination of thin-layer chromatography (TLC) on a chip and surface enhanced Raman scattering (SERS) spectroscopy was used to isolate and detect CBZ from complex food samples. Porous stationary phase composed of diatomite biological silica was conducive to SERS enhancement and elution migration.	/	< 2 ppm	Simple and convenient, but low sensitivity	Shen *et al*. (2021)
SERS	An Au@Ag modified metal-organic framework (MOF, ZIF-8) was prepared, and then the composite MOF was fixed on ITO glass to avoid excessive agglomeration of nanoparticles, and the best SERS substrate was designated as ITO-Au@Ag5@ZIF-8 chip, showing high stability and detection sensitivity.	1.0×10^{-9}-1×10^{-5} mol/L	0.2 μg/kg	High stability, but poor functionality	Zhai *et al*. (2020)
Fluorometry	Graphene quantum dots (SER-GQD-His) are reported to provide a unique dual fluorescence emission. Ser-gqd-his was used as optical probe to detect CBZ fluorescence with DNA cycle amplification. And achieve significant signal amplification.	1.0×10^{-16}-1.0×10^{-9} mol/L	6.1×10^{-17} mol/L	Highly sensitive, but low selectivity and complex process	Li *et al*. (2021)
RRS/SERS	Based on $Au@MOF_{ZnC}$, $HAuCl_4$-SO reaction could be catalytically amplified to generate AuNP and generate RRS and SERS signals. At the same time, combined with Aptc, a new analytical method for detecting CBZ was developed.	0.025-0.5 ng/mL	0.02 ng/mL	Highly sensitive, simple, and fast	This method

Apt_C-$HAuCl_4$-SO-HCl-$Au@MOF_{ZnC}$ system.

K—Slope of the CBZ-Apt_C-$HAuCl_4$-SO-HCl-$Au@MOF_{ZnC}$ system.

$$C=\frac{C_0\times V_0}{V} \quad (3)$$

C_0—Reserve solution concentration of CBZ

V_0 Minimum/maximum volume removed from CBZ Reserve solution

3.9 Interference of ions

The effect of coexisting substances in CBZ-Apt_c-$HAuCl_4$-SO-HCl-$Au@MOF_{ZnC}$ system on RRS/SERS detection of

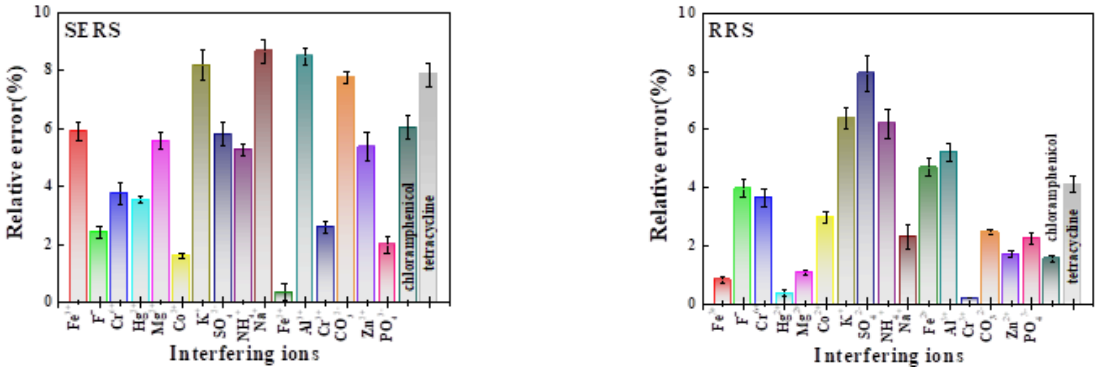

(a) Interference of ions in SERS (b) Interference of ions in RRS

Fig. 9 Interference of ions in SERS and RRS

Table 3 Determination results of CBZ samples

Sample	Single value (ng/mL)	Average (ng/mL)	Added (ng/mL)	Found (ng/mL)	Recovery (%)	RSD (%)	Content
Wastewater 1	0.09, 0.08, 0.09, 0.09, 0.08	0.09	0.03/ 0.05	0.12/ 0.14	97.91/ 101.88	6.37	8.98 ug/mL
Wastewater 2	0.15, 0.13, 0.13, 0.13, 0.14	0.14	0.03/ 0.05	0.17 /0.19	107.28/ 97.20	6.58	1.41 ug/mL
Soil 1	0.24, 0.24, 0.24, 0.23, 0.25	0.24	0.03/ 0.05	0.27 /0.29	101.11 /101.41	2.95	0.97 μg/kg
Soil 2	0.05, 0.05, 0.05, 0.06, 0.05	0.05	0.03/ 0.05	0.07/ 0.10	93.17 /106.95	5.53	0.02 μg/kg
Soil 3	0.04, 0.05, 0.05,0.06, 0.05	0.05	0.03/ 0.05	0.08/ 0.10	102.21/ 92.32	9.27	0.21 μg/kg

0.2 ng/mL CBZ was investigated by experimental method, and the relative error was within ±10 %. For SERS detection system, 100 times of F^-, Mg^{2+}, Co^{2+}, SO_4^{2-}, Al^{3+}, CO_3^{2-}, chloramphenicol and tetracycline, and 10 times of Fe^{3+}, Cr^{6+}, Hg^{2+}, K^+, NH^{4+}, Fe^{2+}, Na^+ and Zn^{2+} had no interference on CBZ determination. (see Figs. 9(a) and 9(b))

3.10 Sample determination

To verify the reliability of the analytical method, the wastewater from a sewage treatment plant, a factory, forest park, mining area and restored area after water treatment in Guilin city were measured. (Liang *et al*. 2021) The CBZ-Apt_c-$HAuCl_4$-SO-HCl-Au@MOF_{ZnC} system was selected to carry out 5 tests on the actual samples, and the average values of the 5 tests were taken as the results. No samples were used as blank control, and the labeling method was further used for testing. According to the table, the relative standard deviation of samples was within 10%, and the recovery rate was between 92.3-107.3%, with good recovery rate and stability. (see Table 3)

4. Conclusions

The Au@MOF_{ZnC} with high catalytic activity and high stability were prepared in this paper. RRS/SERS/Abs spectrum were used to study the catalytic performance of Au@MOF_{ZnC} on the system of $HAuCl_4$-SO. It was found that MOF doped gold nanoparticles could significantly improve the catalytic performance of the system, and could be used as a good dispersant and negative carrier to solve the problem of instability of gold nano sol. A simple, sensitive, and accurate RRS/SERS method for the determination of CBZ and OTC in water and soil was established by using the strategy of catalytic amplification and the adaptor to regulate the catalytic performance.

Acknowledgments

The research described in this paper was financially supported by the National Natural Science Foundation of China. (No. 21767004)

References

Alanazi, F., Almugbel, R., Maher, H.M., Alodaib, F.M. and Alzoman, N.Z. (2021) "Determination of tetracycline, oxytetracycline and chlortetracycline residues in seafood products of Saudi Arabia using high performance liquid chromatography–Photo diode array detection", *Saudi Pharm. J.*, **29**(6), 566-575. https://doi.org/10.1016/j.jsps.2021.04.017.

Ali, M., Esmaeil, H.B., Mohammad, M.F. and Marziyeh, M. (2022), "Electrochemical aptasensor for ultrasensitive detection of PCB77 using thionine-functionalized MoS_2-rGO nano-hybrid", *Microchem. J.*, **155**, 104747. https://doi.org/10.1016/j.microc.2020.104747.

Anshul, Y., Raj Vardhan, P., Bipin, G.V., Pawan, K.L. and Vinod, K.S. "Recovery of CaSO4 and NaCl from sub-soil brine using CNT@MOF5 incorporated poly(vinylidene fluoride-hexafluoropropylene) membranes via vacuum-assisted distillation", *Colloid. Surfaces A.*, **645**, 128918. https://doi.org/10.1016/j.colsurfa.2022.128918.

Bahreyni, A., Luo, H.L., Ramezani, M., Alibolandi, M., Soheili, V., Danesh, N.M., Ashjaei, M.S., Abnous, K. and Taghdisi, S.M. (2020), "A fluorescent sensing strategy for ultrasensitive detection of oxytetracycline in milk based on aptamer-magnetic bead conjugate, complementary strand of aptamer and

PicoGreen", *Spectrochimica Acta A*, **246**, 119009. https://doi.org/10.1016/j.saa.2020.119009.

Deng, H.M., Cai, X.J., Ji, Y., Yan, D., Yang, F., Liu, S.S., Deji, Z.M., Wang, Y., Bian, Z.Y., Tang, G.L., Fan, Z.Y. and Huang, Z.Z. (2022), "Development of a lateral flow immunoassay for rapid quantitation of carbendazim in agricultural products", *Microchem. J.*, **10**, 107495. https://doi.org/10.1016/j.microc.2022.107495.

Dong, W.F., Yang, L.Y. and Huang, Y.M. (2017), "Glycine post-synthetic modification of MIL-53(Fe) metal-organic framework with enhanced and stable peroxidase-like activity for sensitive glucose biosensing", *Talanta*, **167**, 359-366. https://doi.org/10.1016/j.talanta.2017.02.039.

Gaurang, M.P., Jigneshkumar, V.R., Singhal, R.K. and Kailasa, S.K. (2015), "Recognition of carbendazim fungicide in environmental samples by using 4-aminobenzenethiol functionalized silver nanoparticles as a colorimetric sensor", *Sensor. Actuat. B Chem.*, **206**, 684-691. https://doi.org/10.1016/j.snb.2014.09.095.

Gheitaran, R., Afkhami, A. and Madrakian, T. (2022), "PVP-coated silver nanocubes as RRS probe for sensitive determination of Haloperidol in real samples", *Spectrochimica Acta A*, **272**, 121025. https://doi.org/10.1016/j.saa.2022.121025.

Ghorbani, A., Ojani, R., Ganjali, M.R. and Raoof, J. (2021), "Direct voltammetric determination of carbendazim by utilizing a nanosized imprinted polymer/MWCNTs-modified electrode", *J. Iran. Chem. Soc.*, **18**, 3109-3118. https://doi.org/10.1007/S13738-021-02255-3.

Guselnikova, O., Postnikov, P., Elashnikov, R., Miliutina, E., Svorcik, V., Lyutakov, O. (2019), "Metal-organic framework (MOF-5) coated SERS active gold gratings: A platform for the selective detection of organic contaminants in soil", *Analytica Chimica Acta*, **1068**, 70-79. https://doi.org/10.1016/j.aca.2019.03.058.

Harrison, D.L., Patrick, S.W. and Christina, C. (2021), "Metal-organic frameworks for drug delivery: A design perspective", *ACS Appl. Mater. Interf.*, **13**(6), 7004-7020. https://doi.org/10.1021/acsami.1c01089.

Li, C.M., Huang, J.P., Zhu, H.L., Liu, L.L., Feng, Y.M., Hu, G. and Yu, X.B. (2017), "Dual-emitting fluorescence of Eu/Zr-MOF for ratiomeric sensing formaldehyde", *Sensor. Actuat. B Chem.*, **253**, 275-282. https://doi.org/10.1016/j.snb.2017.06.064.

Li, R.Y., Jiang, Y.H., Wang, Q.S., Yang, Y.Q., Li, N.N., Sun, X.L. and Li, Z.J. (2021), "Serine, and histidine-functionalized graphene quantum dot with unique double fluorescence emission as a fluorescent probe for highly sensitive detection of carbendazim", *Sensor. Actuat. B Chem.*, **343**, 130099-130108. https://doi.org/10.1016/J.SNB.2021.130099.

Liang, A.H., Zhi, S.F., Liu, Q.W., Li, C.N. and Jiang, Z.L. (2021), "A new covalent organic framework of dicyandiamide-benzaldehyde nanocatalytic amplification SERS/RRS aptamer assay for ultratrace oxytetracycline with the nanogold indicator reaction of polyethylene glycol 600", *Biosensors*, **11**, 458-458. https://doi.org/10.3390/BIOS11110458.

Ma, C.H., Zhang, J., Hong, Y.C., Wang, Y.R. and Chen, X. (2015), "Determination of carbendazim in tea using surface enhanced Raman spectroscopy", *Chinese Chem. Lett.*, **26**, 1455-1459. https://doi.org/10.1016/j.cclet.2015.10.015.

Sakda, J., Jirachaya, P., Weena, S., Nanthika, K., Nattaya, N., Orawon, C. and Sudkate, C. (2020), "'Signal-On' electrochemical biosensor based on a competitive immunoassay format for the sensitive determination of oxytetracycline", *Sensor. Actuat. B Chem.*, **320**, 128389. https://doi.org/10.1016/j.snb.2020.128389.

Setoudeh, N., Jahani, S., Kazemipour, M., Foroughi, M.M. and Nadiki, H.H. (2020), "Zeolitic imidazolate frameworks and cobalt-tannic acid nanocomposite modified carbon paste electrode for simultaneous determination of dopamine, uric acid, acetaminophen and tryptophan: Investigation of kinetic parameters of surface electrode and its analytical performance", *J. Electroanal. Chem.*, **863**, 114045-114045. https://doi.org/10.1016/j.jelechem.2020.114045.

Shen, Z.D., Fan, Q.Z., Yu, Q., Wang, R., Wang, H. and Kong, X.M. (2021), "Facile detection of carbendazim in food using TLC-SERS on diatomite thin layer chromatography", *Spectrochimica Acta A*, **247**, 119037-119037. https://doi.org/10.1016/j.saa.2020.119037.

Shi, J.L., Li, J.J., Liang, A.H. and Jiang, Z.L. (2022), "Highly catalysis MOF_{Ce} supported Ag nanoclusters coupled with specific aptamer for SERS quantitative assay of trace dopamine", *Talanta*, **245**, 123468. https://doi.org/10.1016/j.talanta.2022.123468.

Shi, P.F., Hu, H.C., Zhang, Z.Y., Xiong, G. and Zhao, B. (2015), "Heterometal-organic frameworks highly sensitive and highly selective luminescent probes to detect I^- ions in aqueous solutions", *Chem. Commun.*, **51**(19), 3985-3988. https://doi.org/10.1039/C4CC09081K.

Shi, X.J., Liu, H.M., Zhang, M., Yang, F.Z., Li, J.S., Guo, Y.M. and Sun, X. (2021), "Ultrasensitive electrochemiluminescence aptasensor based on AuNPs@MWCNTs and Au@AgNPs for detection of profenofos residues", *Sensor. Actuat. B Chem.*, **348**, 130663. https://doi.org/10.1016/J.SNB.2021.130663.

Song, Y., Xie, C.H., Wang, M.S., Liu, S., Zhang, Z.J. and Zhou, Y.B. (2019), "Rapid determination of carbendazim residues in mushrooms by immunosorbent assay", *E3S Web of Conferences*, **78**, 2018-2023. https://doi.org/10.1051/e3sconf/20197802018.

Tawfik, S.M. and Lee, Y.I. (2021), "Metal-organic framework films functionalized with nonionic conjugated polythiophenes for visual detection of PAHs", *Adv. Nano Res.*, **11**(5), 521-536. https://doi.org/10.12989/ANR.2021.11.5.521.

Tayyaba, I., Xu, Y., Ayesha, A., Ghazala, A., Li, G., Muhammad, A., Xiao, F. and Liu, H.F. (2021) "Tuning Electrocatalytic Aptitude by Incorporating α-MnO_2 Nanorods in Cu-MOF/rGO/CuO hybrids: Electrochemical sensing of resorcinol for practical applications", *ACS Appl. Mater. Interf.*, **13**(27), 31462-31473. https://doi.org/10.1021/acsami.1c07067.

Veisi, H., Abrifam, M., Kamangar, S.A., Pirhayati, M., Saremi, S.G., Noroozi, M., Tamoradi, T. and Karmakar, (2021), "B. Pd immobilization biguanidine modified Zr-UiO-66 MOF as a reusable heterogeneous catalyst in Suzuki-Miyaura coupling", *Sci. Rep.*, **11**(1), 21883-21883. https://doi.org/10.1038/S41598-021-00991-3.

Wang, S., Su, L.T., Wang, L.M., Zhang, D.W., Shen, G.Q. and Ma, Y. (2020), "Colorimetric determination of carbendazim based on the specific recognition of aptamer and the poly-diallyldimethylammonium chloride aggregation of gold nanoparticles", *Spectrochimica Part A*, **228**, 117809. https://doi.org/10.1016/j.saa.2019.117809.

Wang, Z.H., Shu, Y.Y., Li, J.J., Liang, A.H. and Jiang, Z.L. (2022), "Silver nanosol RRS aptamer assay of trace glyphosate based on gold-doped polystyrene nanocatalytic amplification", *Microchem. J.*, **176**, 107252. https://doi.org/10.1016/J.MICROC.2022.107252.

Wen, G.Q., Xiao, Y., Chen, S.X., Zhang, X.H. and Jiang, Z.L. (2021), "A nanosol SERS/RRS aptamer assay of trace cobalt (II) by covalent organic framework BtPD-loaded nanogold catalytic amplification", *Royal Soc. Chem.*, **3**, 3846-3859. https://doi.org/10.1039/D1NA00208B.

Wu, J.X. and Yan, B. (2017), "Eu (III)-functionalized In-MOF (In (OH)bpydc) as fluorescent probe for highly selectively sensing organic small molecules and anions especially for $CHCl_3$ and MnO_4^-", *J. Colloid Interf. Sci.*, **504**, 197-205. https://doi.org/10.1016/j.jcis.2017.05.054.

Wu, Z.P., Wang, M.X., Zhou, L.J., Yin, Z.L., Tan, J., Zhang, J.L.

and Chen, Q.Y. (2014), "Framework-solvent interactional mechanism and effect of NMP/DMF on solvothermal synthesis of $[Zn_4O(BDC)_3]_8$", *Transact. Nonferrous Metals Soc. China*, **24**(11), 3722-3731. https://doi.org/10.1016/S1003-6326(14)63521-4.

Yang, Z.C., Liu, T., Wang, W. and Zhang, L.M. (2020), "Stacked hexagonal prism of Ag@Ni-MOF-1 as functionalized SERS platform through rational integration of catalytic synthesis of dopamine-quinone at physiological pH with a biomimetic route", *Chem. Commun.*, **56**(20), 3065-3068. https://doi.org/10.1039/c9cc09145a.

Yao, D.M., Li, C.N., Wang, H.L., Wen, G.Q., Liang, A.H. and Jiang, Z.L. (2020), "A new dual-mode SERS and RRS aptasensor for detecting trace organic molecules based on gold nanocluster-doped covalent-organic framework catalyst", *Sensor. Actuat. B Chem.*, **319**, 128308. https://doi.org/10.1016/j.snb.2020.128308.

Yao, D.M., Li, C.N., Wen, G.Q., Liang, A.H. and Jiang, Z.L. (2020), "A highly sensitive and accurate SERS/RRS dual-spectroscopic immunosensor for clenbuterol based on nitrogen/ silver-codoped carbon dots catalytic amplification-Science Direct", *Talanta*, **209**, 120529-120538. https://doi.org/10.1016/j.talanta.2019.120529.

Yao, D.M., Wen, G.Q., Gong, L.B., Li, C.N., Liang, A.H. and Jiang, Z.L. (2020), "A highly sensitive SERS and RRS coupled di-mode method for CO detection using nanogolds as catalysts and bifunctional probes", *Nanomaterials*, **10**(3), 450-463. https://doi.org/10.3390/nano10030450.

Zhai, Y., Xuan, T., Wu, Y.P., Guo, X.Y., Ying, Y., Wen, Y. and Yang, H.F. (2020), "Metal-organic-frameworks-enforced surface enhanced Raman scattering chip for elevating detection sensitivity of carbendazim in seawater", *Sensor. Actuat. B Chem.*, **326**, 128852-128857. https://doi.org/10.1016/j.snb.2020.128852.

Zhao, J.H., Yuan, H.C., Hong, Q., Peng, Y.J., Li, Y. and Liu, M.H. (2014), "Determination of oxytetracycline content in duck meat using silver nanoparticle enhanced fluorescence", *Opt. Precis. Eng.*, **22**(11), 2902-2907. https://doi.org/10.3788/ope.20142211.2902.

Zheng, D., Hua, X.Z., Fu, X.F., Xia, Z.Z., Zhou, Y.X., Peng, L.J., Yu, Q.W. and Peng, X.T. (2022), "Flowerlike Ni–NiO composite as magnetic solid-phase extraction sorbent for analysis of carbendazim and thiabendazole in edible vegetable oils by liquid chromatography-mass spectrometry", *Food Chem.*, **374**, 131761. https://doi.org/10.1016/j.foodchem.2021.131761.

CC